Electronic Supplementary Information (ESI)

Ag nanoparticles enhancing *Phaseolus vulgaris* seedling development: Understanding nanoparticles migration and chemical transformation across seed coat

Susilaine M. Savassa[a], Hiram Castillo-Michel[b], Ana Elena Pradas del Real[c], Juan Reyes Herrera[b], João Paulo Rodrigues Marques[a], Hudson W. P. de Carvalho[a]

[a.] Laboratory of Nuclear Instrumentation, Centre for Nuclear Energy in Agriculture, University of São Paulo, Piracicaba, SP13416000, Brazil

[b.] European Synchrotron Radiation Facility (ESRF), 38043, Grenoble, Cedex 9, France

[c.] Madrid Institute for Agricultural Research (IMIDRA), N-II km 38,200, 28800 Alcala de Henares, Spain.

Contents

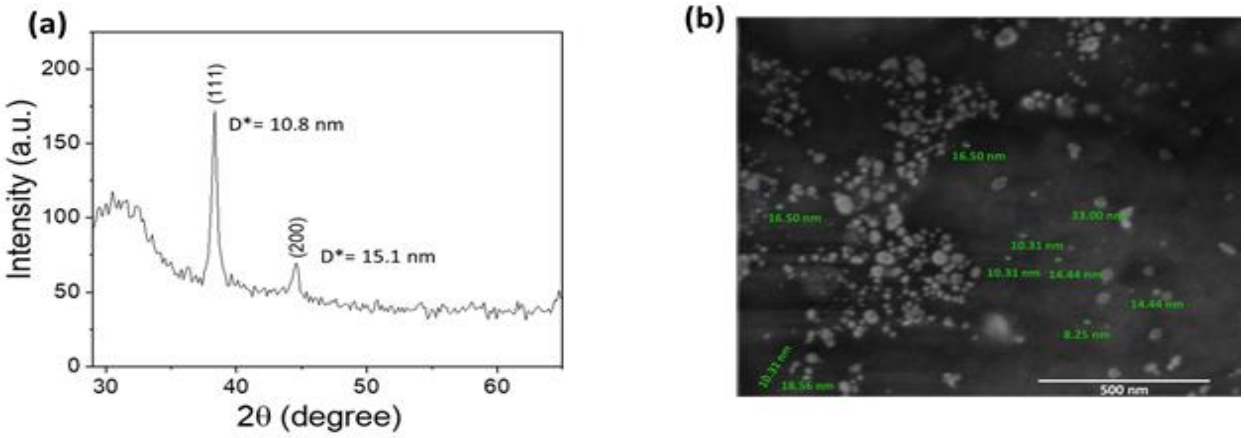

(c)

Dynamic Light Scattering	Zeta Potential
33.6 (± 0.7)	26.4 (± 0.4)

Fig. S1 Ag^0 NP characterization. (a) XRD pattern and crystallite size; (b) Scanning Electron Microscopy (SEM) image and (c) dynamic light scattering (DLS) and Zeta potential.

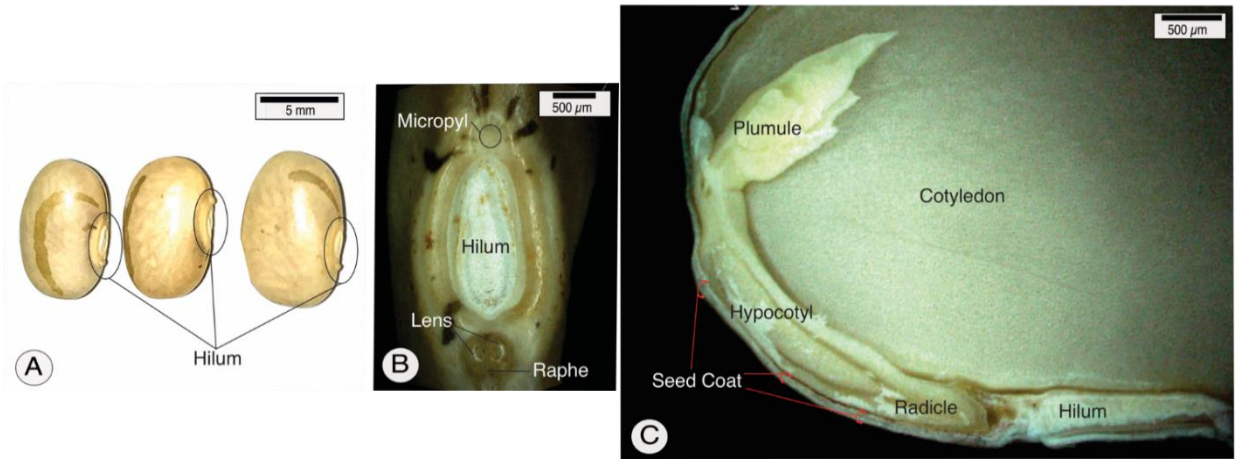

Fig. S2 Common bean (*Phaseolus vulgaris* L.) seed morphology. A. External view of the seeds. B. Detail of the region of the hilum. Note the micropyle, lens and raphe. C. Longitudinal section of the seed. It is possible to observe the embryo with radicle, hypocotyl, cotyledon and plumule. The seed coat cover is thin and cover all the seed.

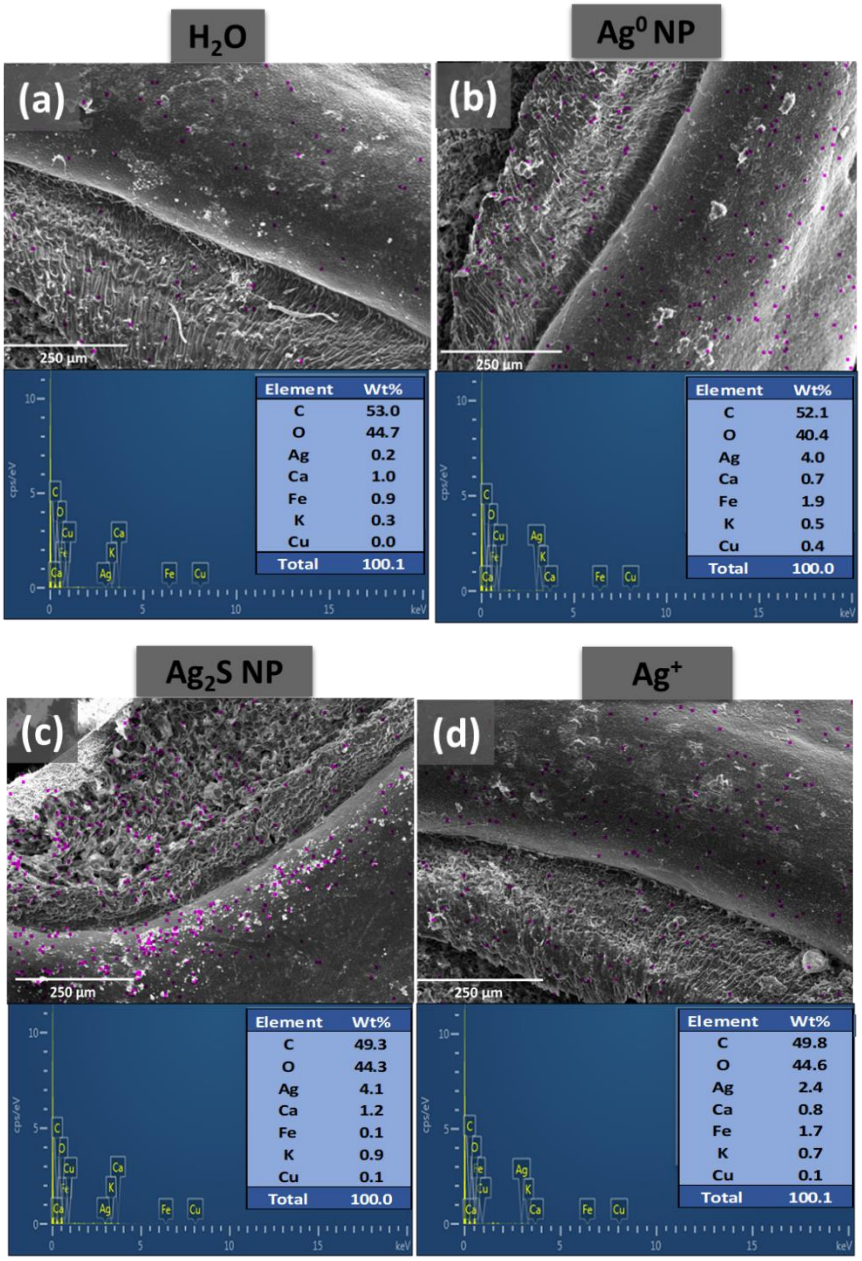

Fig. S3 Scanning electron microscopy (SEM) and energy-dispersive X-ray spectroscopy (EDS) microanalysis for samples treated with (a) H_2O (control), (b) Ag^0 NP, (c) Ag_2S NP and (d) $AgNO_3$. The pink dots represent the regions where the Ag was detected. The seeds were soaked in 1000 mg Ag L^{-1} treatments

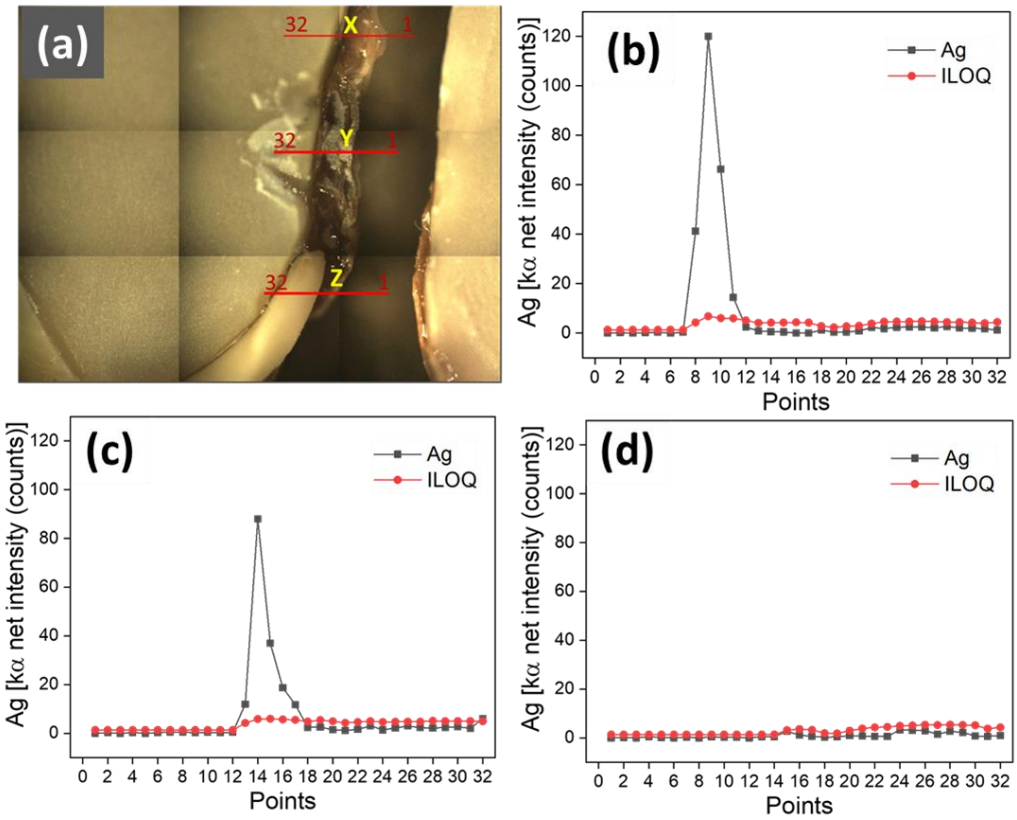

Fig. S4 (a) Picture and Ag line scans of the hilum of common bean (*Phaseolus vulgaris*) sections exposed to Ag_2S NP. Points acquired from (b) X line region, (c) Y line region and (d) Z line region. Black points are the Ag net intensity and red points are the instrumental limit of quantification (ILOQ) for Ag. 1 and 32 indicate the start direction of the acquisition of the points of each analyzed region.

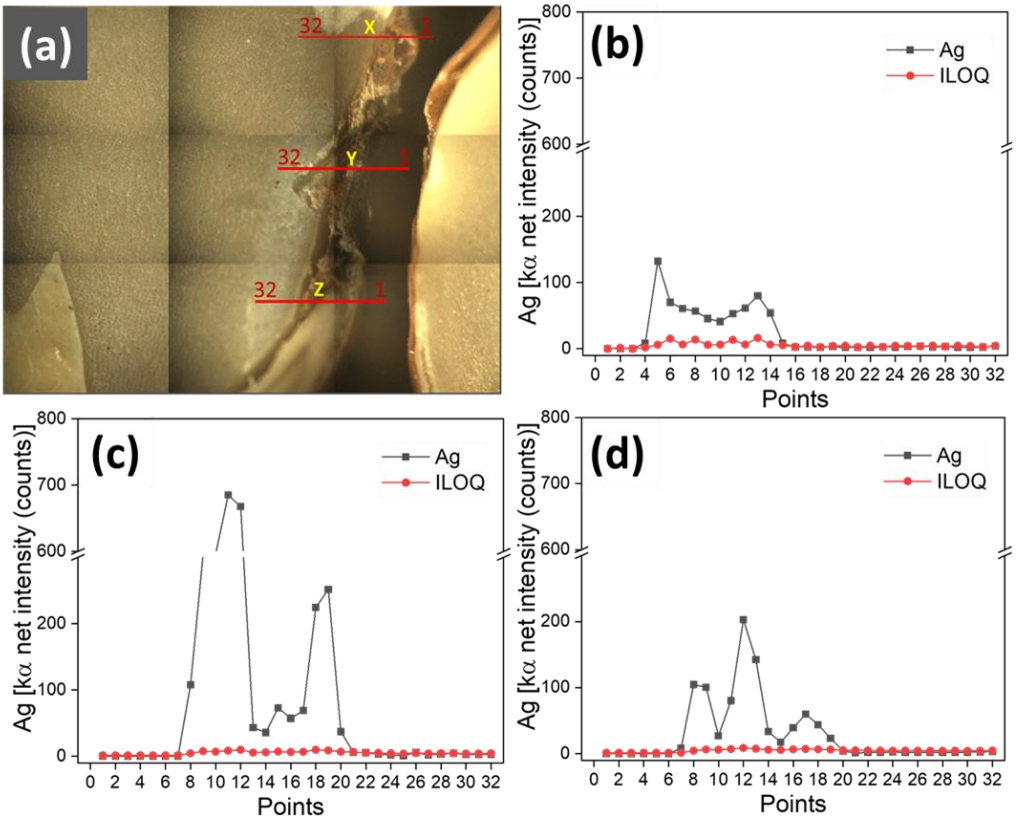

Fig. S5 (a) Picture and Ag line scans of the hilum of common bean (*Phaseolus vulgaris*) sections exposed to Ag^0 NP. Points acquired from (b) X line region, (c) Y line region and (d) Z line region. Black points are the Ag net intensity and red points are the instrumental limit of quantification (ILOQ) for Ag. 1 and 32 indicate the start direction of the acquisition of the points of each analyzed region.

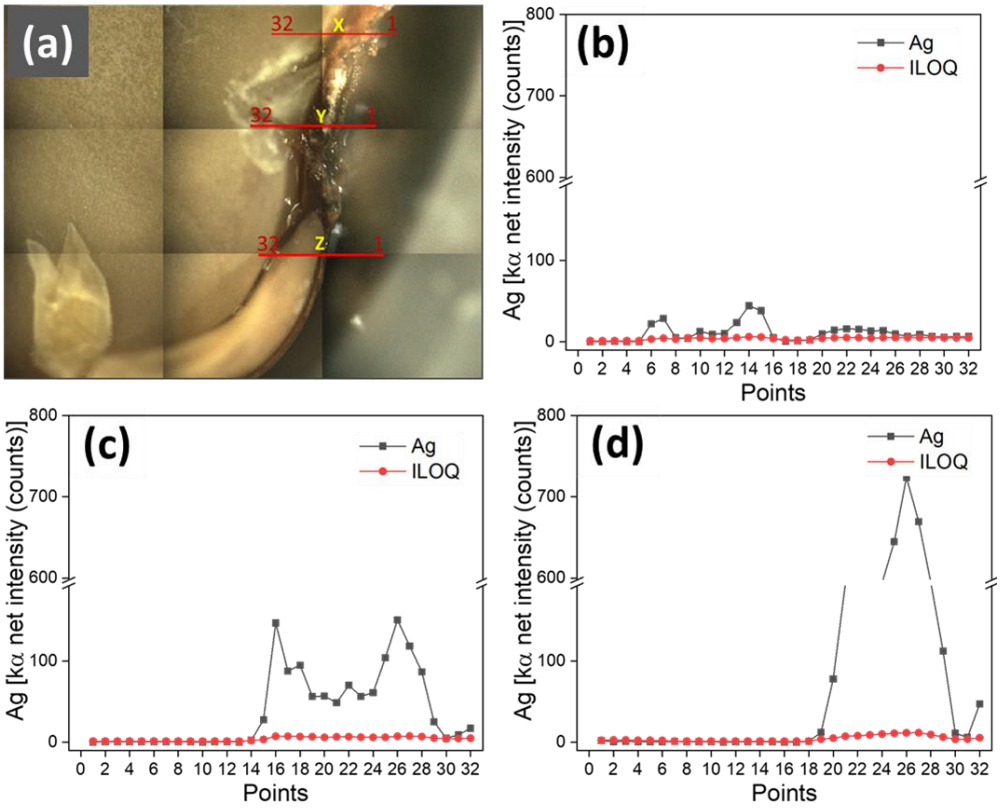

Fig. S6 (a) Picture and Ag line scans of the hilum of common bean (*Phaseolus vulgaris*) sections exposed to $AgNO_3$. Points acquired from (b) X line region, (c) Y line region and (d) Z line region. Black points are the Ag net intensity and red points are the instrumental limit of quantification (ILOQ) for Ag. 1 and 32 indicate the start direction of the acquisition of the points of each analyzed region.

Instrumental Limit of quantification (ILOQ) determination

The ILOQ was determined using the following equation:

$$ILOQ = 10 \times \sqrt{BG}/t$$

ILOQ: Instrumental Limit of Quantification

BG: background measurement

t: Time of spectra acquisition (s)

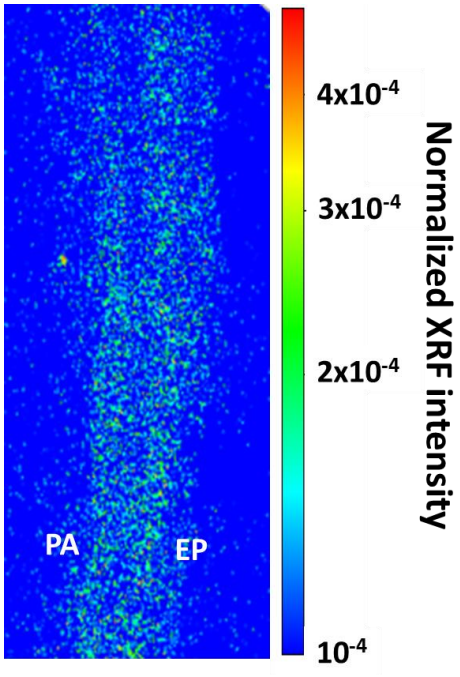

Fig. S7 Control (H_2O) SR-µXRF map showing Ag intensity from cross sections of *Phaseolus vulgaris* seed coat. EP - epidermis, PA – parenchyma layers.

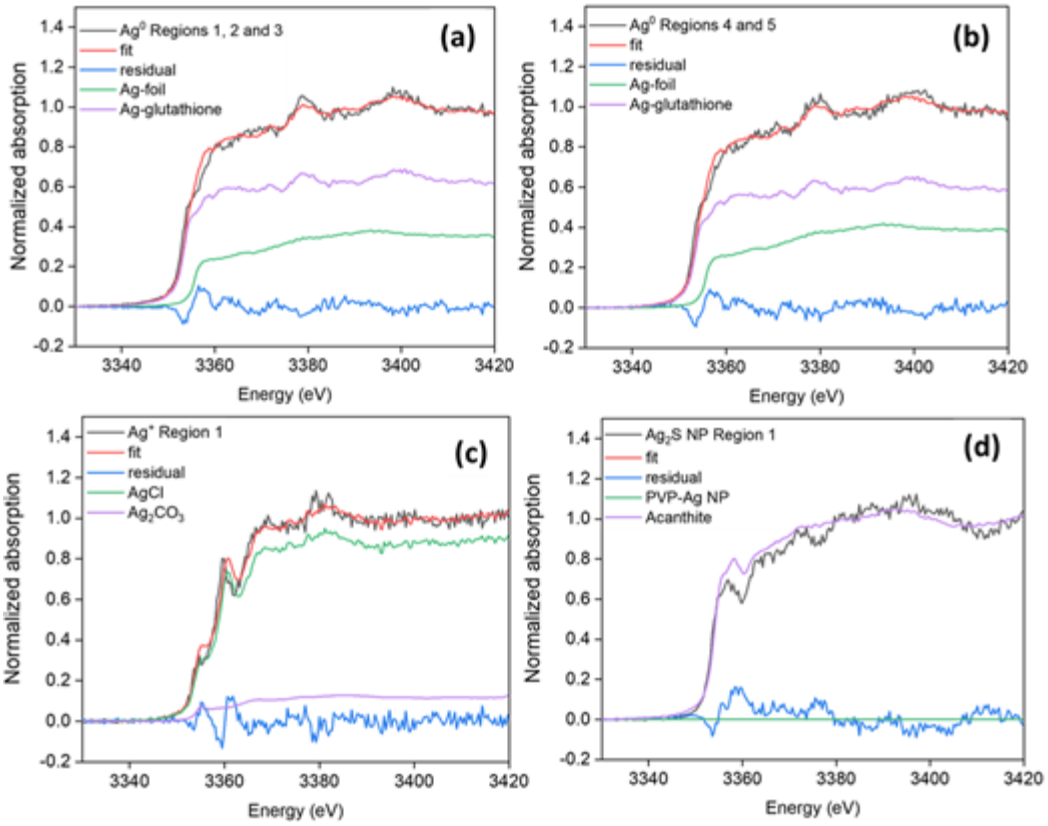

Fig. S8 Linear combination fit for Ag-L edge XAS spectra recorded for (a) regions 1, 2 and 3 from seed coat (Figure 5 main text) from seeds treated with Ag^0 NP (R-factor: 0.0055732, pattern weights: Ag-foil - 0.640, Ag-glutathione 0.360); (b) regions 4 and 5 from seeds treated with Ag^0 NP (R-factor: 0.0053021, pattern weights: Ag-foil - 0.606, Ag-glutathione 0.394); (c) region 1 from seeds treated with $AgNO_3$ (R-factor: 0.0089423, pattern weights: AgCl - 0.882, Ag_2CO_3 0.118) and (d) region 1 from seeds treated with Ag_2S NP (R-factor: 0.0187312, pattern weights: Acanthite - 1.000).

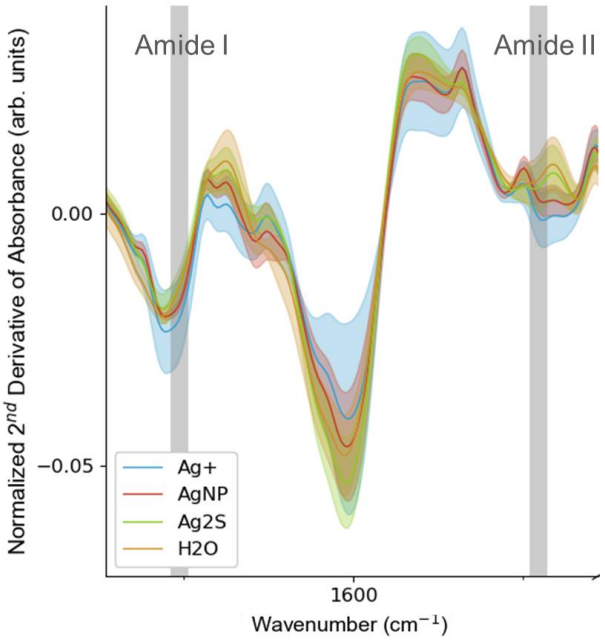

Fig. S9 Mean spectra from internal seed coat surface of common bean seed coat treated samples with weighted Lasso logistic regression coefficients (vertical lines) highlighting the amide I and amide II region. The spectra in these regions are shifted.

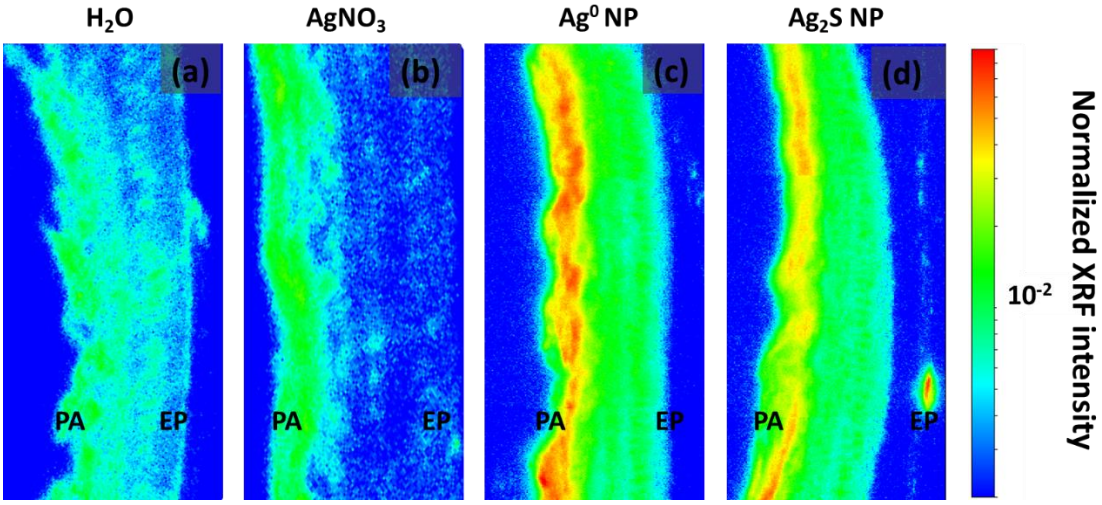

Fig. S10 SR-µXRF maps showing S intensity from cross sections of *Phaseolus vulgaris* seed coat. Seed sections exposed to: (a) Control (H_2O), (b) $AgNO_3$ 100 mg Ag L^{-1}, (c) Ag^0 NP 100 mg Ag L^{-1} and (d) Ag_2S NP 100 mg Ag L^{-1} NP. EP - epidermis, PA – parenchyma layers.

Table S1 The FTIR spectral bands assignment selected by LASSO method for external seed coat samples

Letter	Wavenumber range (cm^{-1})	Attributions	Main Compounds	Ref.
H	873-874	ν(C–O)	β–d-fructose	[4]
G	892	ν(CC), β(CCH)	carbohydrate molecule	[7]
F	1032	ν(C–O), ν(C–C)	Cellulose	[8]
E	1050-1052	C–O–C stretch; C–OH stretch; C–OH deformation; C–O–C deformation	carbohydrate molecule	[6]
E	1055	ν(C–O–C); ν(C–OH); def(C–OH); def(C–O–C)	pyranose, and furanose ring (carbohydrate molecule)	[6]
E	1077	β(COH)	Amylopectin and amylose	[1]
D	1260	ν(C-C), ν(C-O), ν(C=O), ν(C-N), δ(N-H), νas(PO2), ν(P=O)	Lignin, proteins (amide III), and various polysaccharides	[6]
C	1527	Stretching C = N, C = C	Amide groups	[9]
B	1540-1541	ν(C=N); ν(N–H)	Amide II	[4]
A	1627	ν(C=C)	Phenolic compound	[7]

Key: ν - stretching, as – asymmetric, s - symmetric, β – in-plane bending, δ - scissoring, ω - wagging, τ - twisting, def – deformation.

Table S2 The FTIR spectral bands assignment selected by LASSO method for internal seed coat surface samples.

Letter*	Wavenumber range (cm^{-1})	Attributions	Main Compounds	Ref.
I	935 – 998	ν(CO)	C-O-C linkages	[1]
H	1035	ν(OH), ν(C–OH)	Cell wall polysaccharides (arabinan)	[2]
G	1044	ν(C-O), ν(C-C), ν(C=C), ν(COC)	Pectin, various polysaccharides, also suberin or cutin	[3]
F	1507-1509	ν(C=C) aromatic	lignin	[4]
E	1531	δ(NH); ν(CN)	amide II bands of proteins	[5]
D	1607	ν(C=O) aromatic	lignin, alkaloid	[4]
C	1626-1628	C=C stretch	phenolic compound	[4]
B	1661	ν(C=O)	amide I-proteins	[6]
A	1725	ν(C=O), ν(COO^-)	Fatty acids and various polysaccharides	[3]

Key: ν - stretching, as – asymmetric, s - symmetric, β – in-plane bending, δ - scissoring, ω - wagging, τ - twisting.

References

1 M. Kačuráková and M. Mathlouthi, FTIR and laser-Raman spectra of oligosaccharides in water: characterization of the glycosidic bond, *Carbohydr. Res.*, 1996, **284**, 145–157.

2 Y. Zhu and T. L. Tan, Penalized discriminant analysis for the detection of wild-grown and cultivated Ganoderma lucidum using Fourier transform infrared spectroscopy, *Spectrochim. Acta Part A Mol. Biomol. Spectrosc.*, 2016, **159**, 68–77.

3 M. Regvar, D. Eichert, B. Kaulich, A. Gianoncelli, P. Pongrac and K. Vogel-Mikuš, Biochemical characterization of cell types within leaves of metal-hyperaccumulating Noccaea praecox (Brassicaceae), *Plant Soil*, 2013, **373**, 157–171.

4 S. Türker-Kaya and C. Huck, A Review of Mid-Infrared and Near-Infrared Imaging: Principles, Concepts and Applications in Plant Tissue Analysis, *Molecules*, 2017, **22**, 168.

5 J. KONG and S. YU, Fourier Transform Infrared Spectroscopic Analysis of Protein Secondary Structures, *Acta Biochim. Biophys. Sin. (Shanghai).*, 2007, **39**, 549–559.

6 E. Buta, M. Cantor, R. Ştefan, R. Pop, I. Mitre, M. Buta and R. E. Sestraş, FT-IR Characterization of Pollen Biochemistry, Viability, and Germination Capacity in Saintpaulia H. Wendl. Genotypes, *J. Spectrosc.*, 2015, **2015**, 1–7.

7 E. Wiercigroch, E. Szafraniec, K. Czamara, M. Z. Pacia, K. Majzner, K. Kochan, A. Kaczor, M. Baranska and K. Malek, Raman and infrared spectroscopy of carbohydrates: A review, *Spectrochim. Acta Part A Mol. Biomol. Spectrosc.*, 2017, **185**, 317–335.

8 G. Monnier, E. Frahm, B. Luo and K. Missal, Developing FTIR microspectroscopy for analysis of plant residues on stone tools, *J. Archaeol. Sci.*, 2017, **78**, 158–178.

9 A. C. S. Talari, M. A. G. Martinez, Z. Movasaghi, S. Rehman and I. U. Rehman, Advances in Fourier transform infrared (FTIR) spectroscopy of biological tissues, *Appl. Spectrosc. Rev.*, 2017, **52**, 456–506.